Journal of Materials Chemistry B

PAPER

View Article Online
View Journal | View Issue

Cite this: J. Mater. Chem. B, 2014, 2, 4500

pH-activatable near-infrared fluorescent probes for detection of lysosomal pH inside living cells†

Giri K. Vegesna,[a] Jagadeesh Janjanam,[a] Jianheng Bi,[a] Fen-Tair Luo,*[b] Jingtuo Zhang,[a] Connor Olds,[a] Ashutosh Tiwari*[a] and Haiying Liu*[a]

Received 25th March 2014
Accepted 15th May 2014

DOI: 10.1039/c4tb00475b

www.rsc.org/MaterialsB

Four near-infrared fluorescent probes (**A**, **B**, **C** and **D**) have been synthesized, characterized, and evaluated for detection of lysosomal pH inside living cells. The fluorescent probes display highly sensitive and selective fluorescent response to acidic pH as the acidic pH results in drastic structural changes from spirocyclic (non-fluorescent) forms to ring-opening (fluorescent) forms of the fluorescent probes. The fluorescence intensities of the fluorescent probes (**B**, **C** and **D**) increase significantly by more than 200-fold from pH 7.4 to 4.2. The fluorescent probe **D** bearing the *N*-(2-hydroxyethyl) ethylene amide residue possesses the advantages of high sensitivity, excellent photostability, good cell membrane permeability, strong pH dependence, and low auto-fluorescence background. It has been successfully applied to selectively stain lysosomes and detect lysosomal pH changes inside normal endothelial and breast cancer cells.

Introduction

Intracellular pH, known as pH_i, plays a pivotal role in cell function and regulation such as cell volume regulation, vesicle trafficking, cellular metabolism, cell membrane polarity, cellular signaling, cell activation, growth, proliferation and apoptosis.[1–4] Abnormal pH values in organelles are associated with many diseases such as cancer and Alzheimer's.[5,6] A low intra-compartmental pH in organelles functions to denature proteins or activate enzymes that are normally inactive around neutral pH.[7] For example, the membrane around lysosomes at pH 4.5–5.0 enables digestive enzymes to degrade proteins, DNA, RNA, polysaccharides, lipids, viruses and bacteria.[4,7,8] Significant disruptive changes in the lysosomal pH can lead to lysosome malfunction and consequently result in lysosomal storage diseases.[9] Therefore, it is very important to precisely monitor lysosomal pH inside living cells in order to investigate cellular functions and understand physiological and pathological processes. A variety of techniques such as microelectrodes, nuclear magnetic resonance,[10] absorbance spectroscopy, and fluorescence imaging and spectroscopy[11–22] have been developed to measure intracellular pH. Fluorescence spectroscopy using pH-sensitive fluorescent probes is becoming one of the most powerful tools for monitoring intracellular pH, and possesses many technical and practical advantages over other methods because it can detect the intracellular pH of intact cells and subcellular regions with operational simplicity, high sensitivity, and excellent spatial and temporal resolution.[11–21] Although several fluorescent probes for pH have been developed,[23] only a few of them have been applied to detect lysosomal pH inside living cells. Most fluorescent probes including the commercial ones take advantages of lysosomotropism where their weak bases of tertiary amine groups help the probes selectively accumulate in acidic lysosomes through the protonation of the amine groups in a cellular acidic environment.[18] Their pH sensitivity primarily results from protonation of ionizable tertiary amine groups on the fluorophores in acidic lysosomes enhancing the probe fluorescence through the suppression of photo-induced electron transfer from the tertiary amine to the probe fluorophores.[15] The potential drawback for these fluorescent probes is their broad pH response and relative high fluorescent background at pH 7.4. In order to address the fluorescent background issue, a few fluorescent probes for pH based on fluorescein and Rhodamine dyes have been developed to take advantages of low fluorescence background at pH 7.4 because spirolactam rings of the fluorophores exists in the "ring-closed" state at pH 7.4.[12,13,20,24] However, some fluorescent probes can result in cell damage because of their short absorption and emission wavelengths with less than 600 nm. In this paper, we report four near-infrared fluorescent probes (**A**, **B**, **C** and **D**) with spirocyclic structures which are highly sensitive to the pH changes of the solutions. We chose four different residues of fluorescent probes in order to investigate effect of hydrophobic and hydrophilic residues on the cell imaging experiments. The

[a]Department of Chemistry, Michigan Technological University, Houghton, MI 49931, USA. E-mail: hyliu@mtu.edu; tiwari@mtu.edu

[b]Institute of Chemistry, Academia Sinica, Taipei, Taiwan 11529, Republic of China. E-mail: luoft@gate.sinica.edu.tw

† Electronic supplementary information (ESI) available: ^{1}H NMR and ^{13}C NMR, absorption and emission spectra of the fluorescent probes, absorption and fluorescent spectra of the fluorescent probes at different pH values, and fluorescent spectra of fluorescent probes at pH 7.0 and 4.1 in the absence and presence of different metal ions, respectively. See DOI: 10.1039/c4tb00475b

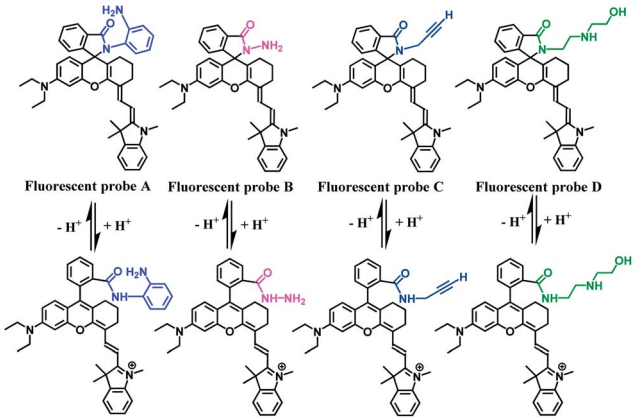

Scheme 1 Spirocyclic ring closing and opening forms of near-infrared fluorescent probes upon pH changes.

fluorescent probes **A** and **C** possess hydrophobic residues such as aminophenyl amide, and ethynyl amide residues while the fluorescent probes **B** and **D** bear hydrophilic residues such as amino amide and *N*-(2-hydroxyethyl) ethylene amide residues, respectively. Under neutral or basic conditions, the fluorescent probes retain the spirocyclic form that is non-fluorescent and colorless. Acidic environment effectively triggers ring opening of the spirocyclic form in fluorescent probes, and results in strong fluorescence (Scheme 1). Three sensitive near-infrared fluorescent probes (**B**, **C** and **D**) have been used to detect lysosomal pH inside living cells with advantages of deep tissue light penetration and low autofluorescence. The fluorescent probes display extremely weak fluorescence at the extracellular pH at 7.4 and become strongly fluorescent at the intracellular lysosomal pH at 4.5. However, the fluorescent probe **A** did not work in cell imaging experiments because of its aminophenyl amide hydrophobic residue.

Experimental section

Instrumentation

^{1}H NMR and ^{13}C NMR spectra were obtained by using a 400 MHz Varian Unity Inova NMR spectrophotometer instrument. ^{1}H NMR and ^{13}C NMR spectra were recorded in $CDCl_3$, chemical shifts (δ) were given in ppm relative to solvent peaks (^{1}H: δ 7.26; ^{13}C: δ 77.3) as internal standard. HRMS were measured with fast atom bombardment (FAB) ionization mass spectrometer, double focusing magnetic mass spectrometer or matrix assisted laser desorption/ionization time of flight mass spectrometer. Infrared (IR) spectra were obtained in the 400–4000 cm^{-1} range using Perkin Elmer Spectrum One FTIR spectrometer. Absorption spectra were taken on a Perkin Elmer Lambda 35 UV/VIS spectrometer. Fluorescence spectra were recorded on a Jobin Yvon Fluoromax-4 spectrofluorometer. Fluorescence spectra of fluorescent probes were measured by using standard 1 cm path-length fluorescence quartz cuvette at room temperature. All samples were scanned with increments of 1 nm. Each spectrum for absorbance and fluorescence was measured at room temperature. 5 μM fluorescent probe solution was used every single time under different pH environment. The citric acid sodium phosphate buffer solution was prepared freshly. The excitation wavelength at 670 nm was used to excite all fluorescent dyes.

Materials

Unless otherwise indicated, all reagents and solvents were obtained from commercial suppliers and used without further purification. Air- and moisture-sensitive reactions were conducted in oven-dried glassware using a standard Schlenk line or drybox techniques under an inert atmosphere of dry nitrogen.

Fluorescent probe A. When phosphorous oxychloride (0.68 g, 4.4 mmol) was added to the compound **5** (0.5 g, 0.89 mmol) in 1,2-dichloroethane (20 mL) under a nitrogen atmosphere, the resulting reaction mixture was refluxed for 4 hours. After the solvent was removed under reduced pressure, dry acetonitrile (30 mL) was added to the reaction residue. When 1,2-diaminobenzene (**6**) (0.38 g, 3.5 mmol) and triethylamine (0.5 mL) was added to the reaction solution, the reaction mixture was stirred at room temperature for overnight. After the solvent was removed under reduced pressure, the reaction residue was dissolved in dichloromethane (50 mL), washed with water (2 × 20 mL) and brine solution (2 × 20 mL), respectively. Organic layer was collected, dried over anhydrous sodium sulfate, filtered and concentrated under reduced pressure. The crude compound was purified by flash column chromatography using EtOAc/hexane (50/50) to yield yellow crystal (0.34 g, 60%). ^{1}H NMR (400 MHz, $CDCl_3$): δ 7.97–7.95 (d, J = 8.0 Hz, 1H), 7.54–7.45 (m, 2H), 7.34–7.31 (d, J = 12.0 Hz, 1H), 7.24–7.22 (d, J = 8.0 Hz, 1H), 7.16–7.11 (m, 2H), 6.99–6.95 (t, J = 8.0 Hz, 1H), 6.83–6.80 (t, J = 8.0 Hz, 1H), 6.66–6.52 (m, 5H), 6.31–6.24 (m, 2H), 5.34–5.31 (d, J = 12.0 Hz, 1H), 3.36–3.31 (q, J = 8.0 Hz, 4H), 3.11 (s, 3H), 2.63–2.57 (m, 1H), 2.38–2.30 (m, 1H), 2.15–2.04 (m, 1H), 1.66–1.61 (m, 7H), 1.37–1.25 (m, 2H), 1.18–1.14 (t, J = 8.0 Hz, 6H). ^{13}C NMR (100 MHz, $CDCl_3$): δ 167.10, 157.65, 153.41, 152.40, 148.97, 148.32, 145.56, 144.14, 139.06, 132.66, 131.63, 128.79, 128.42, 127.88, 127.38, 123.96, 123.54, 123.47, 121.71, 120.85, 119.42, 119.34, 118.93, 118.10, 108.57, 105.85, 104.38, 98.24, 92.24, 70.89, 45.60, 44.54, 29.50, 29.29, 28.66, 28.36, 25.52, 24.60, 23.98, 22.28, 12.76. IR (cm^{-1}): 3346.38, 2968.95, 2928.01, 1681.57, 1619.38, 1592.07, 1493.12, 1354.13, 1316.93, 1263.72, 1216.24, 1192.80, 1126.33, 1078.00, 1019.85, 930.06, 735.45, 702.26. HRMS (ESI) calcd for $C_{43}H_{45}N_4O_2$ $[M + H]^+$, 649.3542; found, 649.3559.

Fluorescent probe B. After compound **5** (0.30 g, 0.53 mmol) was dissolved in dry dichloromethane (30 mL) under nitrogen atmosphere at room temperature, dicyclohexylcarbodiimide (DCC) (0.10 g, 0.53 mmol), and 4-dimethylaminopyridine (0.007 g, 0.06 mmol) were added to the reaction mixture at room temperature. When hydrazine hydrate (0.2 mL, 6.25 mmol) was added to the mixture, the reaction mixture was stirred for 60 minutes at room temperature. Workup procedure was the same as that for fluorescent probe **A**. The crude compound was purified by flash column chromatography using EtOAc/Hexane (50/50) to get a yellow solid (0.15 g, 50%). ^{1}H NMR (400 MHz, $CDCl_3$): δ 7.89–7.87 (d, J = 8.0 Hz, 1H), 7.49–7.40 (m, 3H),

7.19–7.13 (m, 3H), 6.86–6.79 (m, 1H), 6.60–6.59 (m, 1H), 6.39–6.26 (m, 3H), 5.37–5.34 (d, $J = 12.0$ Hz, 1H), 3.64 (brs, 2H), 3.36–3.31 (q, $J = 8.0$ Hz, 4H), 3.13 (s, 3H), 2.60–2.43 (m, 2H), 1.93–1.89 (m, 1H), 1.71–1.69 (m, 6H), 1.36–1.24 (m, 3H), 1.18–1.14 (t, $J =$ 8.0 Hz, 6H). ^{13}C NMR (100 MHz, $CDCl_3$): δ 166.50, 157.96, 153.45, 149.82, 148.99, 148.75, 145.55, 139.05, 132.50, 131.01, 128.42, 127.91, 123.66, 123.17, 121.73, 120.32, 119.86, 119.49, 108.61, 105.88, 104.29, 102.93, 98.17, 92.22, 68.02, 49.20, 45.64, 44.59, 34.19, 30.26, 30.14, 29.33, 28.58, 28.50, 25.87, 25.55, 25.19, 23.20, 22.50, 12.78. IR (cm^{-1}): 2929.64, 1700.81, 1622.93, 1595.03, 1517.70, 1493.73, 1318.14, 1264.97, 1128.16, 735.27, 702.01. HRMS (ESI) calcd for $C_{37}H_{41}N_4O_2$ $[M + H]^+$, 573.3229; found, 573.3247.

Fluorescent probe C. When compound **5** (0.30 g, 0.53 mmol) was dissolved in dry dichloromethane (20 mL) under nitrogen atmosphere at room temperature, *N*-hydroxy-succinimide (0.08 g, 0.69 mmol), dicyclohexylcarbodiimide (DCC) (0.11 g, 0.53 mmol) were added to the reaction mixture sequentially. After 30 minutes stirring, propargylamine (0.04 g, 0.80 mmol) was added through a syringe under nitrogen atmosphere and the reaction mixture was stirred at room temperature for 2 hours. After the reaction mixture was washed with water (2 × 20 mL), the organic layer was collected, dried over anhydrous sodium sulfate and filtered. The filtrate was concentrated under reduced pressure. The crude compound was purified by flash column chromatography using EtOAc/Hexane (25/75) to afford pale yellow syrupy compound (0.19 g, 60%). ^{1}H NMR (400 MHz, $CDCl_3$): δ 7.89–7.87 (d, $J = 8.0$ Hz, 1H), 7.50–7.39 (m, 3H), 7.20–7.14 (m, 3H), 6.88–6.79 (m, 1H), 6.65–6.53 (m, 1H), 6.34–6.24 (m, 3H), 5.44–5.27 (m, 1H), 4.24–4.19 (dd, $J = 16.0$, 4.0 Hz, 1H), 3.76–3.71 (dd, $J = 16.0$, 4.0 Hz, 1H), 3.36–3.31 (q, $J = 8.0$ Hz, 4H), 3.20–3.03 (brs, 3H), 2.67–2.30 (m, 2H), 2.01–1.95 (m, 1H), 1.75–1.70 (m, 6H), 1.61–1.24 (m, 4H), 1.18–1.15 (t, $J = 8.0$ Hz, 6H). ^{13}C NMR (100 MHz, $CDCl_3$): δ 167.79, 153.26, 148.97, 132.66, 131.56, 128.70, 128.36, 127.97, 123.67, 123.26, 121.76, 119.55, 108.67, 105.93, 104.59, 97.99, 79.28, 70.43, 45.66, 44.60, 28.66, 25.56, 24.62, 23.43, 22.19, 12.81. IR (cm^{-1}): 3303.82, 2981.38, 1699.76, 1501.13, 1393.66, 1368.38, 1250.46, 1146.75, 1049.46, 855.42, 736.62, 702.53. HRMS (FAB) calcd for $C_{40}H_{42}N_3O_2$ $[M]^+$, 596.3277; found, 596.3276.

Fluorescent probe D. After 1,1′-carbonyldiimidazole (**9**) (0.06 g, 0.4 mmol) was added to the solution of compound **5** (0.15 g, 0.26 mmol) in anhydrous dichloromethane (20 mL) under nitrogen atmosphere, the reaction mixture was stirred at room temperature for 4 hours. After the complete consumption of compound **5** (confirmed by TLC), *N*-(2-hydroxyethyl)ethylenediamine (0.05 mL, 0.53 mmol) was added to the mixture, the reaction mixture was further stirred overnight. After work-up, the organic layer was washed with water (2 × 30 mL) and brine solution (2 × 30 mL), respectively, dried over anhydrous sodium sulfate, and filtered. The filtrate was concentrated under reduced pressure. The crude compound was purified by preparative TLC plate with dichloromethane/EtOH (20/1) to afford a brown solid (0.09 g, 52%). ^{1}H NMR (400 MHz, $CDCl_3$): δ 7.81–7.79 (d, $J = 8.0$ Hz, 1H), 7.49–7.34 (m, 3H), 7.16–7.09 (m, 3H), 6.81–6.77 (t, $J = 8.0$ Hz, 1H), 6.57–6.55 (d, $J = 8.0$ Hz, 1H), 6.35–6.23 (m, 3H), 5.37–5.34 (d, $J = 12.0$ Hz, 1H), 3.53–3.26 (m, 8H), 3.10 (s, 3H), 2.67–2.38 (m, 6H), 1.72–1.60 (m, 7H), 1.39–1.23 (m, 3H), 1.16–1.12 (t, $J = 8.0$ Hz, 6H). ^{13}C NMR (100 MHz, $CDCl_3$): δ 169.13, 157.96, 152.96, 151.81, 148.90, 148.26, 145.50, 138.99, 132.42, 132.04, 128.60, 128.36, 127.93, 123.62, 123.01, 121.72, 120.27, 119.87, 119.55, 108.66, 107.87, 105.93, 105.46, 103.60, 97.95, 92.24, 67.24, 61.06, 51.17, 48.14, 45.65, 44.57, 40.03, 30.58, 30.16, 29.89, 29.32, 28.71, 28.52, 25.55, 23.25, 22.44, 12.78. IR (cm^{-1}): 3364.27, 2968.80, 2927.21, 1682.60, 1621.06, 1592.96, 1515.14, 1492.83, 1466.55, 1352.63, 1316.87, 1264.54, 1214.76, 1192.54, 1125.75, 1077.46, 929.65, 817.77, 733.88, 701.34. HRMS (ESI) calcd for $C_{41}H_{49}N_4O_3$ $[M + H]^+$, 645.3804; found, 645.3823.

Cell culture and confocal fluorescence imaging

Breast cancer (MDA-MB-231) and normal endothelial (HUVEC-C) cell lines were obtained from ATCC. The cells were cultured according to the published procedures.[25] Briefly, the cells were plated on 12-well culture plates or 35 mm glass bottom culture dishes (MatTek Corp.) at a density of 1×10^5 cells per mL for live cell imaging. After 24 h incubation at 37 °C in 5% CO_2 incubator, the media was removed and cells were rinsed with 1× PBS. Fresh serum free media with 5 or 20 μM of fluorescent probes **A**, **B**, **C**, **D**, and **5** were added and incubated for 2 hours. Live cell imaging was performed with inverted fluorescence microscope (Model AMF-4306; $EVOS_{fl}$, AMG) for initial dye concentration standardization. The final cell images were obtained with confocal laser scanning microscope (Olympus FV1000) with excitation wavelengths at 405 nm for Hoechst 33342 (Sigma-Aldrich), at 488 nm for LysoSensor Green DND-189 (Invitrogen), and at 635 nm for fluorescent probes **A**, **B**, **C**, **D**, and **5**. The fluorescence images were obtained at 60× magnification and the exposure times for each laser were kept constant for each image series.

MTS assay

MDA-MB-231 cell lines were procured from ATCC. The cells were cultured as described previously.[25] Briefly, the cells were plated on 96-well culture plates at a density of 5000 cells per well. After incubating the cells for 4 h to attach to the surface fresh media with different concentrations (0, 5, 25 and 50 μM) of probes **A**, **B**, **C**, **D** and **5** with 0.5% ethanol were added to the wells. Each sample concentrations were repeated with 6 replicates. The plates were incubated at 37 °C in an incubator with 5% CO_2 for 72 h. MTS assay was performed as described previously.[26]

Results and discussion

Design and synthesis of near-infrared fluorescent probes for pH

Fluorescent dye (**5**) ((*E*)-2-(2-(9-(2-carboxyphenyl)-6-(diethylamino)-2,3-dihydro-1*H*-xanthen-4-yl)vinyl)-1,3,3-trimethyl-3*H*-indol-1-ium perchlorate) was chosen as a near-infrared fluorophore to prepare near-infrared fluorescent probes for lysosomal pH in living cells because of its advantageous photophysical properties including a large absorption extinction coefficient

(1.4×10^5 M^{-1} cm^{-1}), high fluorescence quantum yield (41% in methanol) with near-infrared emission peak at 720 nm, good photostability and chemical stability.[27] It displays absorption maximum peak at 710 nm due to $S_0 \rightarrow S_1$ transition, a shoulder peak at 650 nm, and near-infrared emission peak at 731 nm in ethanol mixed solution (please see Fig. S24 and S25 in ESI†). Fluorescent dye (**5**) was prepared by condensation of 2-(4-(diethylamino)-2-hydroxybenzoyl)benzoic acid (**1**) with cyclohexanone (**2**) in acidic conditions, yielding 9-(2-carboxyphenyl)-6-(diethylamino)-1,2,3,4-tetrahydroxanthylium perchlorate (**3**), and followed by condensation of compound **3** with Fisher's aldehyde (**4**) in acetic anhydride at 50 °C (Scheme 2).[27] Near-infrared fluorescent probes were readily synthesized from fluorescent dye **5** through one- or two-step procedures. Fluorescent probe **A** was synthesized by treating fluorescent dye **5** with phosphoryl chloride ($POCl_3$), and followed by further reaction with 1,2-diaminobenzene. Fluorescent probe **B** was prepared by coupling fluorescent dye **5** with dicyclohexylcarbodiimide (DCC) and 4-dimethylaminopyridine (DMAP) in dichloromethane for 30 minutes, and followed by further reaction with hydrazine hydrate for one hour. Fluorescent probe **C** was synthesized by coupling fluorescent dye **5** with *N*-hydroxysuccinimide in the presence of dicyclohexylcarbodiimide (DCC) for 30 minutes, and followed by further reaction with propargylamine (Scheme 2). Fluorescent probe **D** was prepared by reacting fluorescent dye **5** with 1,1′-carbonyldiimidazole (**9**) in dry dichloromethane for four hours, and followed by further reaction with *N*-(2-hydroxyethyl)ethylenediamine for overnight. Introduction of *N*-(2-hydroxyethyl)ethylenediamine to fluorescent dye **5** is expected to enhance hydrophilic property of fluorescent probe and facilitate selective accumulation of fluorescent probe **D** in lysosome of living cells *via* protonation of the secondary amine in an acidic environment at pH 4.5 inside lysosome.

Optical responses of fluorescent probes to pH

We investigated effect of pH on absorption spectra of the fluorescent probes. Fluorescent probe **A** displays a strong absorption peak at 379 nm, a moderate absorption at 479 nm, and an extremely weak absorption peak at 720 nm in 40 mM citrate–phosphate buffer solution containing 40% ethanol at pH 7.48 (Fig. 1A). Gradual decrease of pH from pH 7.0 to pH 4.0 results in significant absorbance enhancement at 720 nm accompanying with a shoulder peak at 663 nm (Fig. 1A and B), indicating that the spirolactam ring of the fluorophore was opened, leading to significant extension of π-conjugation of the fluorophore. Consequently, the solution of the fluorescent probe **A** displays distinct color changes from colorless to green along with the pH titration from 6.9 to 4.0. However, further decrease of pH below 2.0 causes decrease in the absorbance of fluorescent probe **A** at 720 nm (Fig. 1A). This may be due to charge imbalance of the fluorophore as the tertiary amine group of the fluorophore becomes protonated at extremely low pH (Scheme 3). Fluorescent probe **A** displays full fluorescent reversible responses between pH 3.0 and 7.2 when it is treated

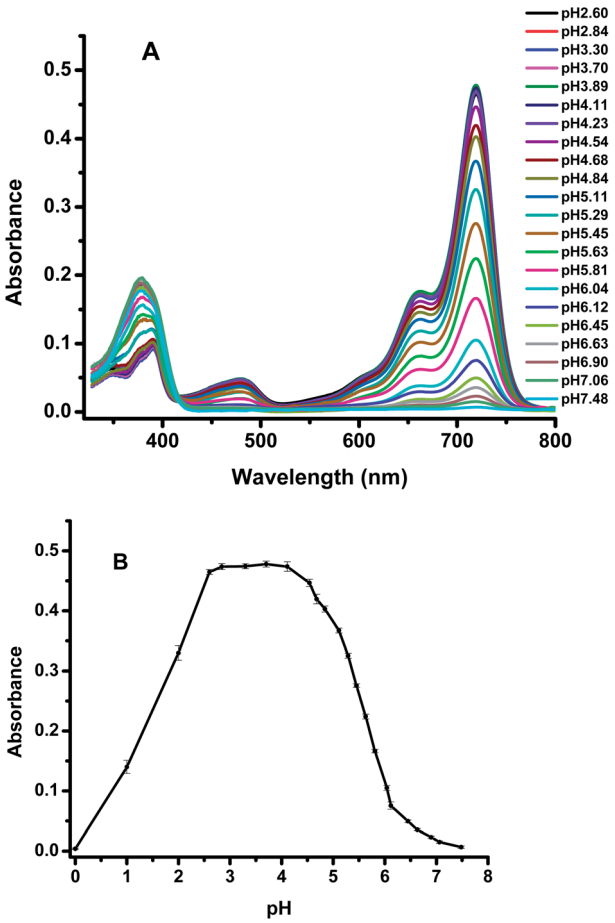

Fig. 1 Absorption spectra of 5 μM fluorescent probe **A** at different pH values in 40 mM citrate–phosphate buffer solution containing 40% ethanol (A) and effect of pH on absorbance of the fluorescent probe **A** at 718 nm with three-repeated measurements (B).

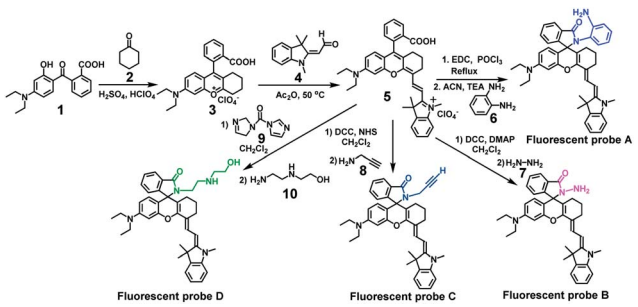

Scheme 2 Synthetic routes to near-infrared fluorescent probe for pH.

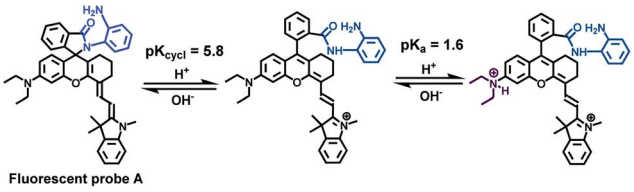

Scheme 3 Chemical structures of fluorescent probe **A** at different pH values.

with acid or base. The similar pH effect on absorbance of fluorescent probes **B**, **C** and **D** were also observed (Fig. 2, and S17–S19 in ESI†).

In order to evaluate fluorescent probes for pH sensing application, we investigated pH effect on fluorescence intensity of 5 μM fluorescent probes in 40 mM citrate–phosphate buffer solution containing 40% ethanol. Fig. 3 displays the fluorescence spectra of fluorescent probe **A** at different pH values. The probe was non-fluorescent when the buffer pH is greater than 7.4. However, gradual decrease of pH from pH 7.4 to pH 4.0 results in appearance of a new fluorescence peak at 743 nm, and significantly enhances fluorescence peak intensity. There is more than 71-fold increase in the fluorescence intensity of fluorescent probe **A** at 743 nm with pH decrease from 7.4 to 4.1, indicating the probe is very sensitive to acidic pH because of the H^+-induced spirolactam ring opening of the fluorophore. In addition, there are slightly red shifts of the fluorescence peak with pH decrease from 7.4 to 4.1, which may be due to enhanced π-conjugation of the fluorescent probe **A** during these pH changes. The pK_{cycl} value of the probe **A** is 5.8 related to spirolactam ring opening, which was obtained according to the Henderson–Hasselbach-type mass action equation. The

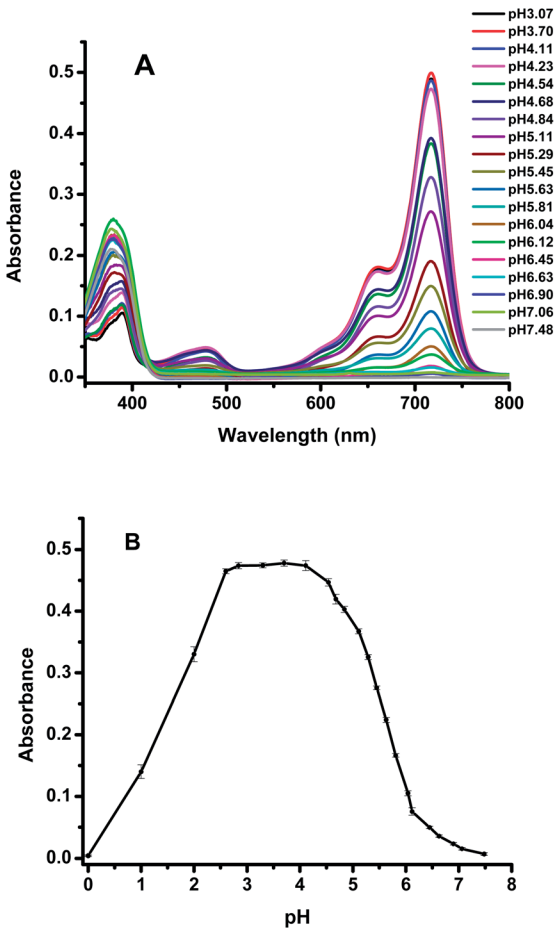

Fig. 2 Absorption spectra of 5 μM fluorescent probe D at different pH values in 40 mM citrate–phosphate buffer solution containing 40% ethanol (A) and effect of pH on absorbance of the fluorescent probe D at 718 nm (B).

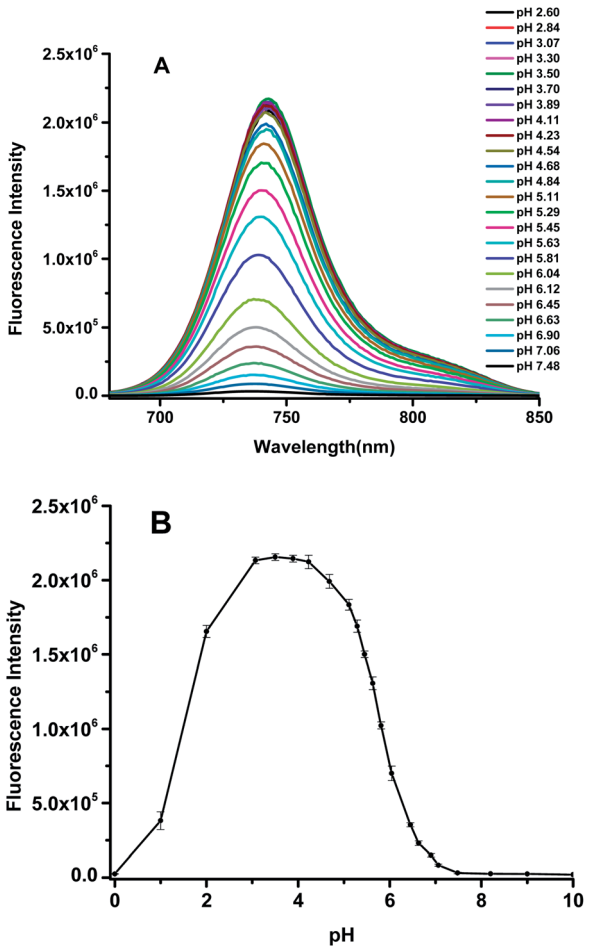

Fig. 3 Fluorescent spectra of 5 μM fluorescent probe A at different pH values in 40 mM citrate–phosphate buffer solution containing 40% ethanol (A) and pH effect on fluorescence intensity of fluorescent probe A at 743 nm with three repeated measurements (B).

fluorescence intensity of the probe **A** displayed linear responses to pH values in the range from 4.9 to 6.6. In addition, it showed excellent reversible responses to pH between 4.0 and 7.4. Compared with fluorescent probe **A**, fluorescent probes **B**, **C** and **D** exhibit much more sensitive fluorescent responses to pH with 395-, 592- and 229-fold increases in the fluorescence intensity at 743 nm with pH decrease from 7.4 to 4.1, respectively. The pK_{cycl} values of the probe **B**, **C** and **D** related to the spirolactam ring opening are 4.6, 4.9 and 5.4, respectively, which indicates that the probes **B**, **C** and **D** are more suitable for lysosome imaging application. However, further decrease of pH to strong acidic conditions triggers significant fluorescence decreases of fluorescent probe **A** because the protonation of the nitrogen atom of the fluorophore significantly reduces the electron donating ability of the nitrogen atom, and results in charge imbalance through the resonance structure (Scheme 3). The analysis of fluorescence intensity changes of fluorescent probe **A** as a function of pH by using the Henderson–Hasselbach-type mass action equation yielded pK_a value of 1.8. The similar pH effect on fluorescent probes **B**, **C** and **D** were also observed with further decrease of pH to strong acidic conditions. The analysis

of fluorescence intensity changes of fluorescent probes **B**, **C** and **D** gave almost the same pK_a value of 1.7 (Fig. 4).

Effect of ethanol amount on fluorescent responses of the fluorescent probes to pH

We studied effect of ethanol amount on fluorescent responses of the fluorescent probes to pH. As the fluorescent probes are not completely soluble in aqueous solution, organic solvent such as ethanol is needed to add to the buffer solution in order to dissolve the probes. An increase of ethanol concentration in the buffer solution enhances fluorescence intensity of the fluorescent probe **D** as the probe solubility become improved with an increase of ethanol concentration in 40 mM citrate–phosphate buffer solution (Fig. 5). The similar results were observed in the fluorescent probes **A**, **B** and **C** (Fig. S17, S21 and S25 in ESI†).

The selectivity experiments of fluorescent probes to pH over metal ions

We investigated effect of metal ions on fluorescent response of fluorescent probes to pH by evaluating potential coordination of fluorescent probes with heavy, transition, and main group metal ions (Fig. 6). Fluorescent probes **A**, **B**, **C** and **D** display no responses to 200 μM alkali and alkaline-earth metal ions such as Na^+, K^+, Ca^{2+} and Mg^{2+}, as well as some transitional metal ions (200 μM) such as Cu^{2+}, Zn^{2+}, Fe^{3+}, Fe^{2+}, Co^{2+}, Ag^+, Ba^{2+}, Cd^{2+}, Pb^{2+}, Ni^{2+} and Mn^{2+} at pH 7.0 and 4.1 (Fig. 6, and S27–S29 in ESI†), which indicates that the fluorescent probes display high selectivity to pH over these alkali, alkaline-earth metal ions, and transitional metal ions.

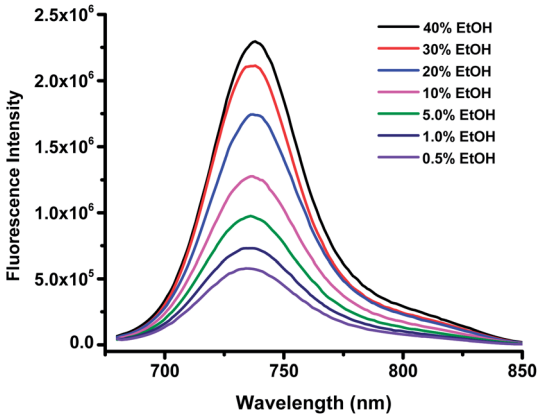

Fig. 5 Fluorescent spectra of 5 μM fluorescent probe **D** in 40 mM citrate–phosphate buffer solution at pH 4 containing different concentrations of ethanol.

Photostability of the fluorescent probes

Fluorescent probes were excited continuously at their optimal excitation for 5 min intervals and fluorescence intensity was measured every 5 min. The result in Fig. 7 clearly shows that the fluorescent probe **D** displays good photostability with its fluorescence decrease by 3.8% under one-hour excitation. The fluorescence intensity of fluorescent probes **A** and **C** decrease by 5.2% and 10.6% under one-hour excitation (Fig. S18 and S26 in ESI†). However, the fluorescent probe **B** shows poor photostability as its fluorescence intensity decreased by 44% under one-hour excitation (Fig. S22 in ESI†).

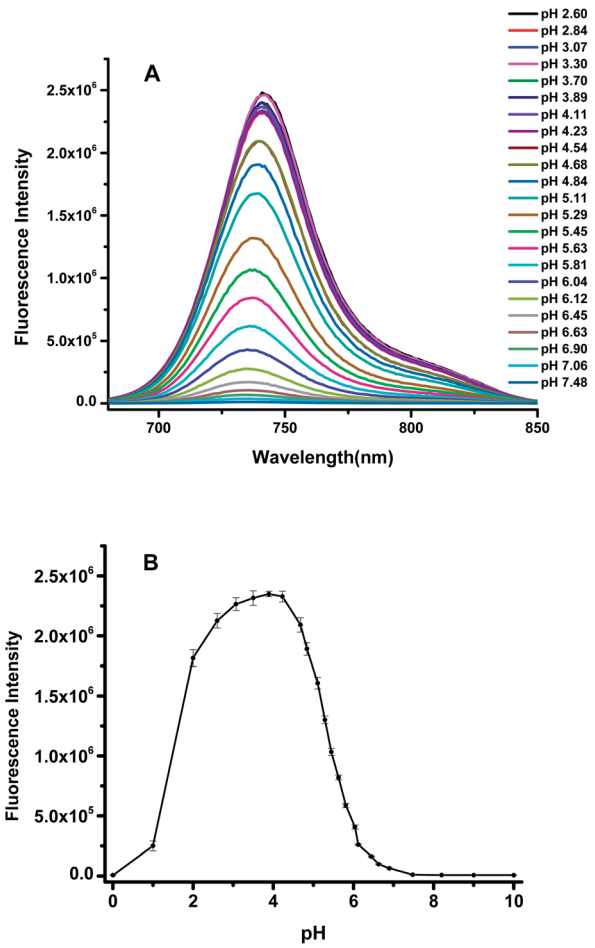

Fig. 4 Fluorescent spectra of 5 μM fluorescent probe **D** at different pH values in 40 mM citrate–phosphate buffer solution containing 40% ethanol (A) and pH effect on fluorescence intensity of fluorescent probe **D** at 743 nm (B).

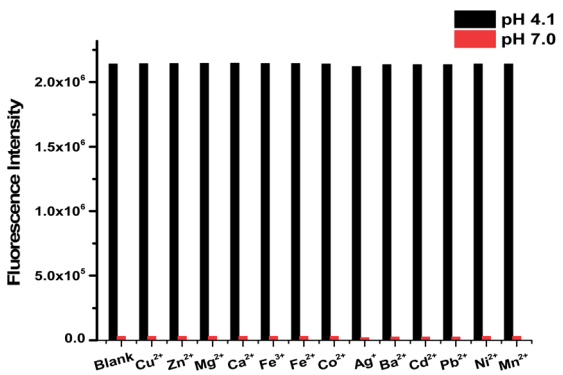

Fig. 6 Fluorescent responses of 5 μM fluorescent probe **A** to pH at 4.1 and 7.0 in the absence and presence of different metal ions (200 μM), respectively.

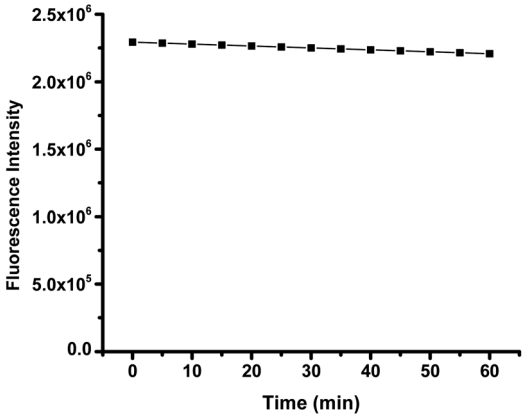

Fig. 7 Photostability of 5 μM fluorescent probe **D** at pH 4.1 in 40% ethanol solution. Sample was exposed under respective optimal excitation wavelength and fluorescence intensities were measured at 5 min intervals.

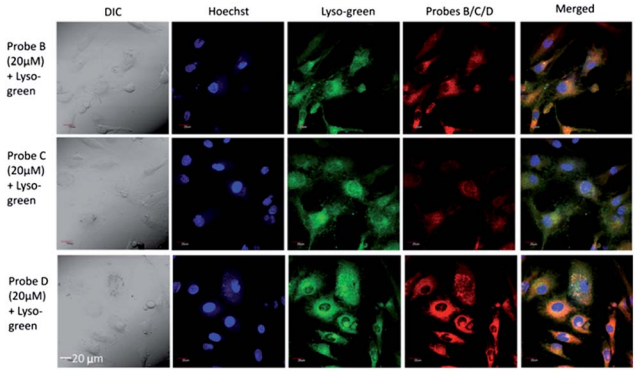

Fig. 9 Fluorescence images of HUVEC-C cells incubated with fluorescent probes **B**, **C**, and **D**. Cells were incubated with 20 μM of all three dyes for 2 h and imaged for co-localization with 5 μM LysoSensor Green and Hoechst stains. The images were acquired using confocal fluorescence microscope at 60× magnification.

Live cell imaging of fluorescent probes

All four fluorescent probes were used as near-infrared fluorescent probes in cultured cells and compared to commercial LysoSensor Green DND-189 and probe **5** to investigate if these probes could be used to target lysosomes/acidic organelles inside the cells as LysoSensor Green DND-189 is known to be retained specifically in acidic organelles. A series of experiments were performed: a breast cancer line (MDA-MB-231) and normal endothelial cell line (HUVEC) were loaded with fluorescent probes **A**, **B**, **C** and **D** and with LysoSensor Green DND-189 (Fig. 8 and 9), respectively. All the probes except probe **A** showed a fluorescence signal inside the cell, specifically localized in lysosomes with maximum signal with probe **D** followed by probe **B** (Fig. 8–10). The fluorescence signals of these probes were compared with the commercially available and well characterized lysosome specific probe, LysoSensor Green DND-189 (Lyso-green). To confirm the co-localization of these probes to lysosomes, we incubated both the cells with Lyso-green and these new probes. Images were captured for the same image field with different excitation and emission wavelengths of near-infrared fluorescent probes as compared to those of probe DND-189, which enables simultaneous visualization of both probes (near-infrared probes and DND-189) from the same intracellular compartment. When the images were overlaid they showed co-localization in lysosomes (Fig. 8–10). The probe **D** was most fluorescent and showed a very high signal even at 5 μM concentration and was clearly co-localized to lysosomes (Fig. 10). The fluorescence intensity of the probe **D** is close to probe DND-189 as the areas of low and high fluorescence of the probe match those of the probe DND-189, indicating the probe **D** can effectively distinguish between different pH values in the cell in a similar manner to the commercial probe DND-189. Probe **B** showed a slightly weaker signal when compared to probe **D** (Fig. 8 and 9). The close-up of co-localization of cells image clearly shows that the lysosomes were mostly localized as perinuclear clusters both in cancer and normal cell lines (Fig. 10). These results are consistent with a previous report that showed lysosomes in serum-starved cells relocate towards the perinuclear position and forms clusters.[28] In this study, the probes were incubated in serum-free media thus the lysosomes localize to perinuclear clusters. This data also confirms that the

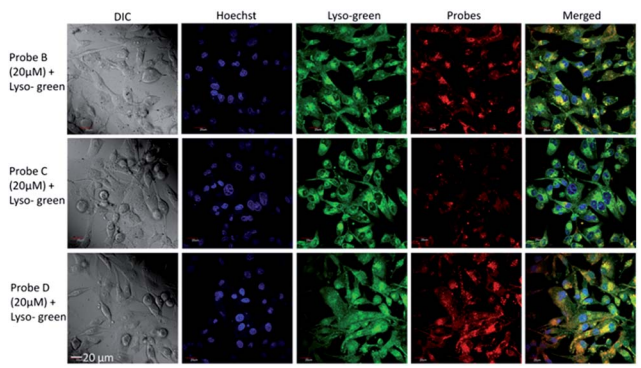

Fig. 8 Fluorescence images of MDA-MB-231 cells incubated with fluorescent probes **B**, **C**, and **D**. Cells were incubated with 20 μM of dyes **B**, **C**, and **D** for 2 h and imaged for co-localization in presence of 5 μM LysoSensor Green, a lysosomal stain and Hoechst, a nuclear stain. The images were acquired using confocal fluorescence microscope at 60× magnification.

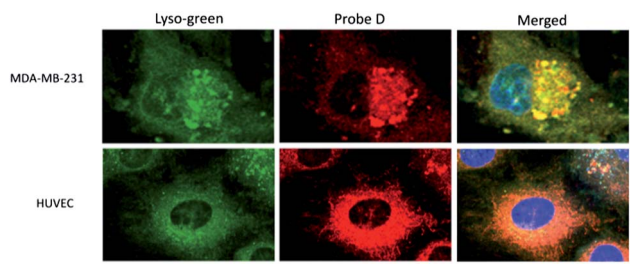

Fig. 10 Enlarged images of MDA-MB-231 and HUVEC-C cells with fluorescent probe **D** showing co-localization of fluorescent probe **D** in lysosomes. The probe **D** shows much stronger signal in HUVEC cells compared to MDA-MB-231 cell. The lysosomes are mostly perinuclear in both cells due to serum-starvation for 2 hours.

probes are localized only in lysosomes and are highly sensitive to pH environment. These fluorescent probes **B**, **C**, and **D** were compared with their precursor probe **5** (Scheme 2) and tested for co-localization (Fig. 11) and cell toxicity (Fig. 12). Probe **5** shows non-specific distribution in cell and stains lysosomes as well as other parts of the cell (Fig. 11). In addition, probe **5** is very toxic and shows >30% cell toxicity for MDA-MB-231 cells at 5 μM concentration compared to nearly 100% viability observed for cells in presence of probes **B**, **C**, and **D** at the same concentration (Fig. 12).

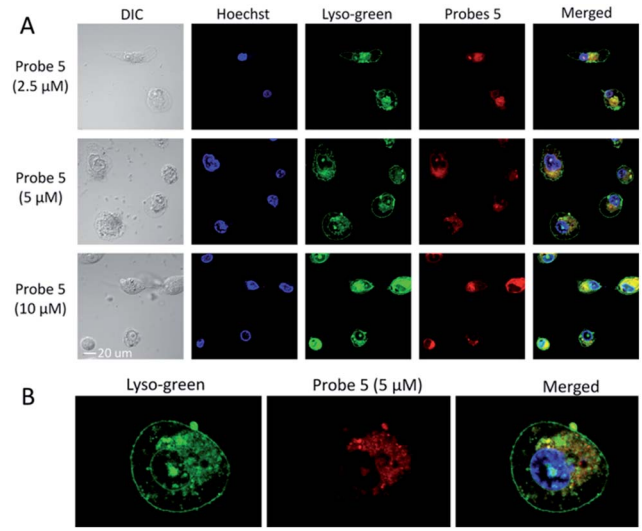

Fig. 11 Fluorescence images of MDA-MB-231 cells incubated for 1 h with 2.5, 5.0, and 10.0 μM concentrations of probe **5**. Cells were imaged for co-localization with LysoSensor Green and Hoechst stains (A). Enlarged image (B) shows localization of probe **5** is not specific to lysosomes. The images were acquired using confocal fluorescence microscope at 60× magnification.

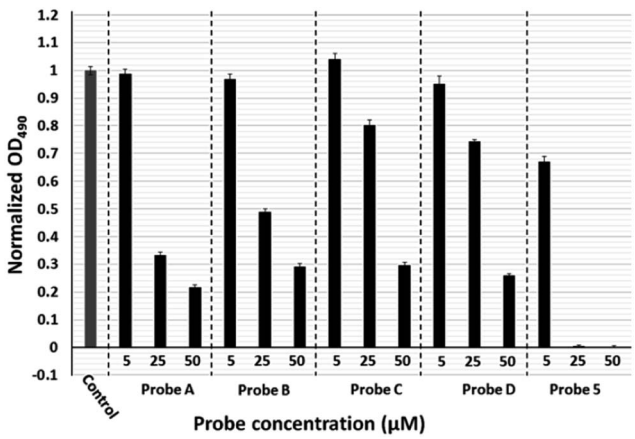

Fig. 12 Cytotoxicity and cell proliferation effect of probes A, B, C, D, and **5** (Scheme 2) were tested by MTS assay. The MDA-MB-231 cells were incubated with 5, 25, and 50 μM concentrations of probes for 72 h and their viability was tested by adding MTS reagent and then reading absorbance at 490 nm for the colored formazon product formed. The absorbance measured at 490 nm is directly proportional to the number of living cells in the culture.

Summary

We have prepared four near-infrared fluorescent probes for pH (**A**–**D**). The response mechanism of the fluorescent probes to pH value relies on the structural changes between spirocyclic and ring-opening forms of the near-infrared fluorophore. These probes are not fluorescent with a spirocyclic form at neutral pH and highly fluorescent with a spirocycle-opening at low pH value of ~4.5. Fluorescent probes have absorption and emission peaks at 718 nm and 743 nm, respectively. The fluorescent probes **B**, **C** and **D** are cell-permeable and are capable of selective and sensitive labeling of lysosomes, and may offer potential noninvasive monitoring of lysosomal pH changes during physiological and pathological processes.

Conflict of interest

The authors declare no competing financial interest.

Acknowledgements

This work was supported partially by National Science Foundation (to H. Y. Liu), ALS Therapy Alliance (to A. Tiwari), and Pruett postdoctoral fellowship support for J. Janjanam (to A. Tiwari).

References

1 S. C. Burleigh, T. van de Laar, C. J. M. Stroop, W. M. J. van Grunsven, N. O'Donoghue, P. M. Rudd and G. P. Davey, *BMC Biotechnol.*, 2011, **11**, 95, DOI: 10.1186/1472-6750-11-95.
2 S. Humez, M. Monet, F. van Coppenolle, P. Delcourt and N. Prevarskaya, *Am. J. Physiol.: Cell Physiol.*, 2004, **287**, C1733–C1746.
3 A. L. Edinger and C. B. Thompson, *Curr. Opin. Cell Biol.*, 2004, **16**, 663–669.
4 A. C. Johansson, H. Appelqvist, C. Nilsson, K. Kagedal, K. Roberg and K. Ollinger, *Apoptosis*, 2010, **15**, 527–540.
5 E. S. Trombetta, M. Ebersold, W. Garrett, M. Pypaert and I. Mellman, *Science*, 2003, **299**, 1400–1403.
6 Y. Urano, D. Asanuma, Y. Hama, Y. Koyama, T. Barrett, M. Kamiya, T. Nagano, T. Watanabe, A. Hasegawa, P. L. Choyke and H. Kobayashi, *Nat. Med.*, 2009, **15**, 104–109.
7 B. Turk and V. Turk, *J. Biol. Chem.*, 2009, **284**, 21783–21787.
8 J. Stinchcombe, G. Bossi and G. M. Griffiths, *Science*, 2004, **305**, 55–59.
9 E. J. Blott and G. M. Griffiths, *Nat. Rev. Mol. Cell Biol.*, 2002, **3**, 122–131.
10 S. He, R. P. Mason, S. Hunjan, V. D. Mehta, V. Arora, R. Katipally, P. V. Kulkarni and P. P. Antich, *Biorg. Med. Chem.*, 1998, **6**, 1631–1639.
11 Z. J. Diwu, C. S. Chen, C. L. Zhang, D. H. Klaubert and R. P. Haugland, *Chem. Biol.*, 1999, **6**, 411–418.
12 H. S. Lv, J. Liu, J. Zhao, B. X. Zhao and J. Y. Miao, *Sens. Actuators, B*, 2013, **177**, 956–963.
13 H. Zhu, J. L. Fan, Q. L. Xu, H. L. Li, J. Y. Wang, P. Gao and X. J. Peng, *Chem. Commun.*, 2012, **48**, 11766–11768.

14 Z. Li, Y. L. Song, Y. H. Yang, L. Yang, X. H. Huang, J. H. Han and S. F. Han, *Chem. Sci.*, 2012, **3**, 2941–2948.
15 L. Q. Ying and B. P. Branchaud, *Bioorg. Med. Chem. Lett.*, 2011, **21**, 3546–3549.
16 D. G. Smith, B. K. McMahon, R. Pal and D. Parker, *Chem. Commun.*, 2012, **48**, 8520–8522.
17 L. J. Ma, W. G. Cao, J. L. Liu, D. Y. Deng, Y. Q. Wu, Y. H. Yan and L. T. Yang, *Sens. Actuators, B*, 2012, **169**, 243–247.
18 F. Galindo, M. I. Burguete, L. Vigara, S. V. Luis, N. Kabir, J. Gavrilovic and D. A. Russell, *Angew. Chem., Int. Ed.*, 2005, **44**, 6504–6508.
19 H. M. DePedro and P. Urayama, *Anal. Biochem.*, 2009, **384**, 359–361.
20 T. Hasegawa, Y. Kondo, Y. Koizumi, T. Sugiyama, A. Takeda, S. Ito and F. Hamada, *Biorg. Med. Chem.*, 2009, **17**, 6015–6019.
21 H. J. Lin, P. Herman, J. S. Kang and J. R. Lakowicz, *Anal. Biochem.*, 2001, **294**, 118–125.
22 J. L. Fan, C. Y. Lin, H. L. Li, P. Zhan, J. Y. Wang, S. Cui, M. M. Hu, G. H. Cheng and X. J. Peng, *Dyes Pigm.*, 2013, **99**, 620–626.
23 J. Y. Han and K. Burgess, *Chem. Rev.*, 2010, **110**, 2709–2728.
24 Z. Q. Hu, M. Li, M. D. Liu, W. M. Zhuang and G. K. Li, *Dyes Pigm.*, 2013, **96**, 71–75.
25 S. L. Zhu, J. T. Zhang, J. Janjanam, J. H. Bi, G. Vegesna, A. Tiwari, F. T. Luo, J. J. Wei and H. Y. Liu, *Anal. Chim. Acta*, 2013, **758**, 138–144.
26 X. Ding, J. Janjanam, A. Tiwari, M. Thompson and P. A. Heiden, *Macromol. Biosci.*, 2014, DOI: 10.1002/mabi.201300569.
27 L. Yuan, W. Y. Lin, Y. T. Yang and H. Chen, *J. Am. Chem. Soc.*, 2012, **134**, 1200–1211.
28 V. I. Korolchuk, S. Saiki, M. Lichtenberg, F. H. Siddiqi, E. A. Roberts, S. Imarisio, L. Jahreiss, S. Sarkar, M. Futter, F. M. Menzies, C. J. O'Kane, V. Deretic and D. C. Rubinsztein, *Nat. Cell Biol.*, 2011, **13**, 453–460.